# NUMERICAL SIMULATION OF FERRITE/AUSTENITE PHASE FRACTION IN MULTIPASS WELDS OF DUPLEX STAINLESS STEELS

T. OGURA*, T. MATSUMURA*, L. YU*, D. C. KIM*,
H. INOUE**, Y. OIKAWA*** and K. SAIDA*

**Dept. of Materials & Manufacturing Science, Osaka University*
*** Joining & Welding Research Institute, Osaka University*
****Nippon Steel & Sumikin Stainless Steel Corporation*

*DOI 10.3217/978-3-85125-615-4-07*

ABSTRACT

Kinetic approach to the α/γ phase transformation phenomena (α/γ phase fraction) in the heat affected zone (HAZ) and weld metal (WM) of multipass welds was made using duplex stainless steels (lean, standard and super duplex stainless steels). The kinetic equations including rate constants of the dissolution behaviour as well as precipitation behaviour of γ phase were determined by isothermal heat treatment test. Based on the kinetic equations determined, the distribution of the γ phase fraction in multipass welds of duplex stainless steels was calculated applying the incremental method combined with the heat conduction analysis during welding. The depleted zone of γ phase was formed adjacent to the fusion line in the base metal HAZs and the reheated WMs. However, the γ phase fraction in the depleted zone was increased (recovered) by the subsequent weld passes. Accordingly, the α/γ phase balance has been complexly varied in multipass welds, and the profile of the γ phase fraction was arranged in laminae in the WM roughly along the fusion lines. Furthermore, the γ phase fraction in multipass weld of standard DSS was slightly lower than those of lean and super DSSs. The over-precipitated zone, where the γ phase fraction slightly exceeded the base metal level, was not observed in the low temperature HAZ of standard DSS weld, whereas it was observed in other welds. Microstructural observation revealed that the calculated results of the γ phase fraction in multipass welds were consistent with experimental ones. It follows that the α/γ phase transformation in duplex stainless steel welds could be successfully predicted by the present approach.

## INTRODUCTION

Duplex stainless steels (DSSs) have been widely applied in various industrial fields such as chemical, energy, food, pharmacy and marine plants. DSSs indicate the dual phase microstructure consisting of the balanced austenitic (γ) and ferritic (α) phases, and possess the superior properties such as high strength and toughness, high corrosion resistance and

good weldability. However, during fusion welding (especially multipass welding), DSSs undergo the complex microstructural change and phase transformation affecting the α/γ phase balance due to a series of thermal cycles [1-4]. The microstructure of the weld metal (WM) is quite different from that of the base metal, *i.e.*, solidified as the single-phase α (F mode) and precipitated the Widmanstätten γ [5]. On the other hand, in the heat affected zone (HAZ), the γ phase fraction is reduced (the α/γ phase balance deviates from the adequate ratio), and Cr-carbides and nitrides and/or intermetallic compounds such as σ and χ phases would be easily precipitated in the γ phase-depleted HAZ [6-9]. As a result, the mechanical and corrosion properties of welds would be seriously deteriorated. It follows that prediction and control of the α/γ phase transformation in DSS welds are required. There are a number of studies concerning the α/γ phase transformation phenomena in DSS welds [5,10-14], while only a few studies have been conducted for investigating the kinetics of the α/γ phase transformation. According to the previous reports, the kinetics of formation (precipitation) of γ phase in the HAZ of DSS welds was followed by the Austin-Rickett type equation [15,16], and the γ phase fraction in the DSS WM was successfully predicted in the cooling thermal cycle with various cooling rates [17]. However, these investigations dealt with only the precipitation phenomena of γ phase in the HAZ under the limited thermal cycles. In particular, the α/γ phase transformation in multipass welds (*i.e.*, multiple thermal cycle) has not been clarified yet. In addition, the dissolution and re-precipitation behaviours of γ phase during thermal cycle were not investigated at all. In the HAZ of DSS welds, γ phase has been dissolved once at the higher temperature in weld thermal cycle, and then precipitated again (re-precipitated) during cooling. In order to predict the α/γ phase transformation in welds, especially multipass welds, it is necessary to clarify the kinetics of dissolution and precipitation of γ phase separately. Furthermore, the precipitation kinetics of γ phase in the WM would differ from that in the HAZ (base metal), because γ phase comes to precipitate in the solidified (solidification-segregated) α structure originated from the F mode solidification.

In the previous studies [18,19], the authors have investigated the kinetics of α/γ phase transformation (dissolution and precipitation behaviours of γ phase) in the HAZ of DSS welds (lean, standard and super DSSs), and the γ phase fraction in the HAZ of single pass melt-run welds was numerically calculated and compared between the types of steel and/or welding techniques. As a result, the dissolution as well as precipitation behaviour of γ phase was followed by the Austin-Rickett type equation, and the rate constants of them involving the temperature dependency were determined for various DSSs. From the fact that the calculated results of the γ phase fraction in the HAZ of gas tungsten arc (GTA) and laser beam (LB) melt-run welds were approximately consistent with experimental ones, the authors have concluded that the α/γ phase transformation in the HAZ of DSS welds could be successfully predicted by the numerical computation. However, the α/γ phase transformation behaviour in the DSS WM has never been predicted in the previous study.

In the multipass welding, the WM as well as HAZ is reheated numerous times by the subsequent weld passes, as a result, the dissolution and/or precipitation of γ phase will alternate in welds. Furthermore, the dissolution and precipitation kinetics of γ phase would differ between in the multipass WM and HAZ (base metal) as pointed out above. Because of such very complicate phase transformation behaviours during multiple thermal cycle, the α/γ phase transformation in multipass DSS welds is hard to predict quantitatively.

In the present study, the kinetic approach was made to the α/γ phase transformation phenomena in the multipass welds of DSSs. Both of the dissolution and precipitation behaviours of γ phase were kinetically investigated for the reheated WM as well as the base metal HAZ, and the γ phase fraction in multipass welds of DSSs was numerically calculated by coupling with the heat conduction analysis during multipass welding. Finally, the predicted results of α/γ phase transformation in multipass welds were verified by the experimental examination.

## MATERIALS AND EXPERIMENTAL PROCEDURES

### MATERIALS

Three types of DSSs, lean, standard and super DSSs, were used for the base metal. Table 1 shows the chemical compositions of the base metals used in this study. A standard and super DSSs are comparable to type 329J3L and 327L1 steels, respectively. All DSSs were heat-treated at 1323 K×5 min after hot rolling. The autogenous filler metals (diameter, 1.2 mm) were used for gas tungsten arc welding (GTAW). The chemical compositions of filler metals are shown in Table 2. The filler metal compositions for lean DSS welding were identical to the base metal compositions (because manufactured from the base metal plate). The γ phase fraction of as-received base metals of DSSs was approx. 50-60%. The dimensions of DSS plates were 50 mm × 70 mm × 4 $mm^t$ (for single pass melt-run welding) and 80 mm × 100 mm × 12 $mm^t$ (for multipass welding).

**Table 1** Chemical compositions of duplex stainless steels used (mass%)

| Steel | C | Si | Mn | P | S | Ni | Cr | Mo | Cu | N | Fe |
|---|---|---|---|---|---|---|---|---|---|---|---|
| Lean DSS | 0.014 | 0.35 | 1.49 | 0.024 | 0.0004 | 3.06 | 20.85 | 0.30 | 0.09 | 0.177 | Bal. |
| Standard DSS | 0.008 | 0.56 | 1.82 | 0.025 | 0.0002 | 5.75 | 22.55 | 3.08 | 0.16 | 0.161 | Bal. |
| Super DSS | 0.009 | 0.31 | 0.51 | 0.024 | 0.0009 | 6.56 | 25.11 | 3.72 | 0.21 | 0.259 | Bal. |

**Table 2** Chemical compositions of filler metals used (mass%)

| Steel | C | Si | Mn | P | S | Ni | Cr | Mo | Cu | N | Fe |
|---|---|---|---|---|---|---|---|---|---|---|---|
| Lean DSS | 0.014 | 0.35 | 1.49 | 0.024 | 0.0004 | 3.06 | 20.85 | 0.30 | 0.09 | 0.177 | Bal. |
| Standard DSS | 0.012 | 0.56 | 1.81 | 0.024 | 0.0005 | 5.72 | 22.46 | 3.07 | 0.17 | 0.169 | Bal. |
| Super DSS | 0.013 | 0.31 | 0.48 | 0.025 | 0.0005 | 6.83 | 24.98 | 4.03 | 0.20 | 0.265 | Bal. |

### EXPERIMENTAL PROCEDURES

In order to manufacture the WM of DSS, single pass melt-run GTAW was carried out using a DSS plate under the welding conditions of arc current, 90 A; arc voltage, 14 A; welding speed, 6 cm/min; shielding gas, Ar+2%$N_2$ (flow rate, 15 L/min). The full weld metal specimen for isothermal heat treatment was machined from the melt-run welded plate. The dimensions of specimen were 3 mm × 8 mm × 1.5 $mm^t$. On the other hand, the base metal specimen for isothermal heat treatment was directly machined from the as-received plate. The dimensions of specimen were 3 mm × 3 mm × 4 $mm^t$.

The isothermal heat treatment of DDS specimen was conducted in the Ar atmosphere using a high frequency induction heating apparatus. The heat-treatment conditions including thermal cycle patterns are summarised in Table 3. Different kinds of isothermal heat treatment were conducted for the kinetic investigation of the dissolution and precipitation phenomena. As for the base metal specimen, the solution treatment at 1373-

**Table 3** Conditions of isothermal heat treatment

| Heat treatment | | Thermal cycle | Conditions | |
|---|---|---|---|---|
| Base metal (Base metal HAZ) | Solution treatment | 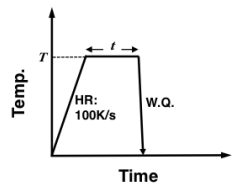 | Heating temp., $T$ | 1373-1633K |
| | | | Holding time, $t$ | 0-3000s |
| | Precipitation treatment | 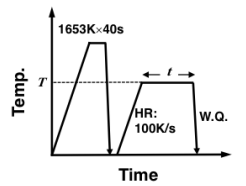 | Heating temp., $T$ | 1073-1423K |
| | | | Holding time, $t$ | 0-3000s |
| Weld metal (Reheated WM) | Solution treatment | 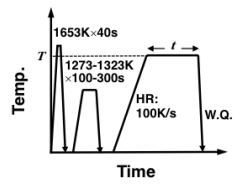 | Heating temp., $T$ | 1473-1623K |
| | | | Holding time, $t$ | 0-30s |
| | Precipitation treatment | 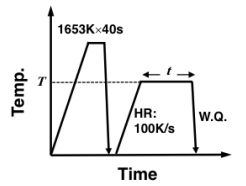 | Heating temp., $T$ | 1123-1423K |
| | | | Holding time, $t$ | 0-1000s |

1633 K for 0-2000 s was performed to investigate the dissolution behaviour of γ phase, and the precipitation treatment at 1073-1423 K for 0-3000 s subsequent to the α single-phasing

treatment (solution treatment) at 1653 K for 40 s was performed to investigate the precipitation behaviour of γ phase in the single-phase α structure. As for the weld metal specimen, the solution treatment at 1473-1623 K for 0-2000 s was performed subsequent to the α single-phasing treatment at1653 K for 40 s and the pre-precipitation treatment at 1273-1323 K for 100-300 s (aimed to the initial amount of γ phase being uniformed at approx. 50%), and the precipitation treatment at 1123-1423 K for 0-1000 s was performed subsequent to the α single-phasing treatment (solution treatment) at 1653 K for 40 s.

The multipass GTAW was carried out for investigation of the microstructure and α/γ phase fraction in welds. The GTAW conditions were as follows: arc current, 160 A; arc voltage, 12 V; welding speed, 12 cm/min (root pass) / arc current, 220 A; arc voltage, 12 V; welding speed, 15 cm/min (other passes); shielding gas, Ar+2%$N_2$ (flow rate, 15 L/min); interpass temp., 373 K; U-groove (angle, 50º; root face, 1 mm).

The microstructure of specimens was observed by an optical microscope (OM) and scanning electron microscope (SEM) after electrolytic etching with a 20%$H_2SO_4$ + methanol solution at 25 V for 40 s. The amount of γ phase (the γ phase fraction) in specimens was measured as the area fraction of γ phase in metallographic structure using the electron back scatter diffraction analysis (EBSD) with OIM crystallography software.

## DISSOLUTION BEHAVIOUR OF AUSTENITIC PHASE

### DISSOLUTION KINETICS IN BASE METAL HEAT AFFECTED ZONE

The change in microstructure of DSSs during the solution treatment was investigated. Fig.1 shows an example of microstructural change (phase mapping by EBSD analysis) in super DSS with the solution treatment condition. The red regions indicate a γ phase, green ones a α phase and yellow ones a σ phase in the microstructure. A typical microstructure of DSS could be observed in all specimens, namely, a γ phase was aligned along the rolling direction. The amount of γ phase decreased with an increase in the heating temperature. Very few σ phase was formed in the present conditions. It has been confirmed that similar dissolution behaviour was observed in lean and standard DSSs. The area fraction of γ phase in the phase map was measured for all steels with varying the heat treatment condition.

In the previous report [18,19], the authors have been reported that the precipitation of γ in steels is followed by the Austin-Rickett type equation as given by eq.(1) or (2) [15,16];

$$\frac{y}{1-y} = (kt)^n \tag{1}$$

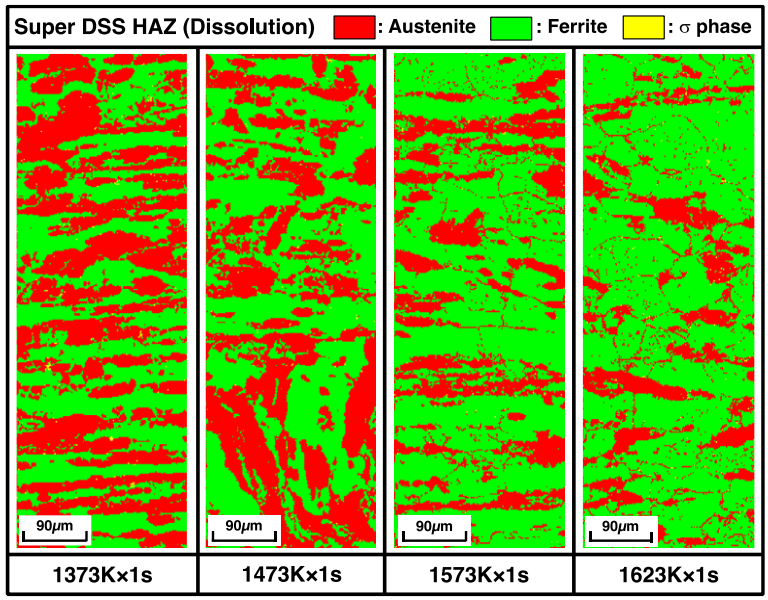


**Fig. 1** Change in microstructure of super DSS with solution treatment

$$\log\frac{y}{1-y} = n\log t + n\log k \tag{2}$$

where $y$ is the fraction transformed, $k$ is the kinetic constant, $t$ is the time and $n$ is the time exponent. Then, applicability of the Austin-Rickett type equation to dissolution phenomena of γ phase was evaluated. Fig.2 shows the Austin-Rickett plot of dissolution behaviour of γ phase in lean, standard and super DSSs (base metal HAZs). There were good linear relationships in the Austin-Rickett plot, and gradients of lines were almost identical independent of the heating temperature. The time exponents, $n$ of lean, standard and super DSSs were determined as 0.49, 0.64 and 0.71, respectively. Consequently, it can be concluded that dissolution kinetics of γ phase in all base metal HAZs of DSSs is followed by the Austin-Rickett type equation.

It has been well-known that the kinetic constant, $k(T)$ can be generally expressed by the Arrhenius type equation as given by eq.(3);

$$k(T) = k_0 \exp\left(-\frac{Q}{RT}\right) \tag{3}$$

where $k_0$ is the frequency factor, $Q$ is the activation energy, $T$ is the absolute temperature and $R$ is the gas constant. The Arrhenius plots of dissolution rate of γ phase in DSSs are shown in Fig.3. There were good linear relationships between ln $k$ and $1/T$ for all steels. Therefore, the temperature dependency of dissolution rate of γ phase in DSSs could be obtained in the present study as follows;

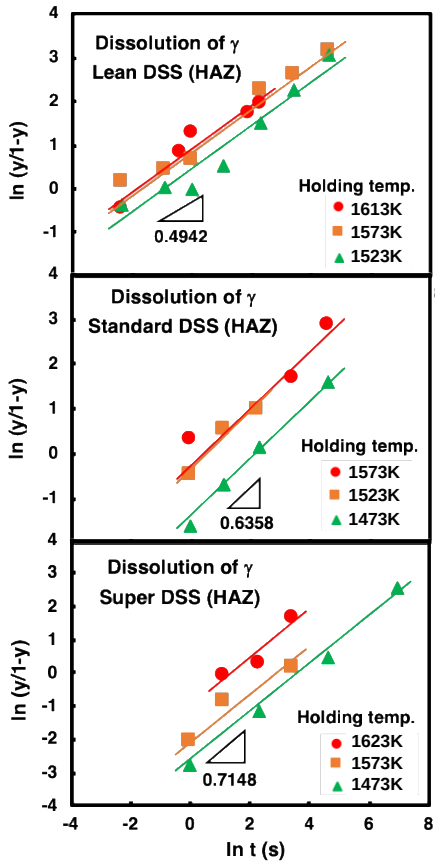


**Fig. 2** Austin-Rickett plots of dissolution behaviour of γ phase in base metal HAZs

Lean DSS HAZ:

$$k(T) = \exp\left(\frac{-2.47\times10^{4}}{T} + 17.2\right) \tag{4}$$

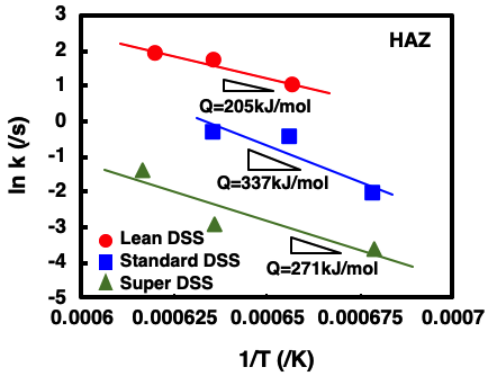


**Fig. 3** Arrhenius plots of dissolution rates of γ phase in base metal HAZs

Standard DSS HAZ:

$$k(T) = \exp\left(\frac{-4.05\times10^4}{T} + 25.6\right) \tag{5}$$

Super DSS HAZ:

$$k(T) = \exp\left(\frac{-3.26\times10^4}{T} + 18.4\right) \tag{6}$$

## DISSOLUTION KINETICS IN REHEATED WELD METAL

As described in INTRODUCTION, the WMs of DSSs are generally solidified as the F mode, and a γ phase comes to precipitate in the solidified α structure during cooling. Then, precipitation kinetics of γ phase was also investigated in the WM (reheated WM). Fig.4 shows the Austin-Rickett plot of dissolution behaviour of γ phase in the WMs of lean, standard and super DSSs. There were good linear relationships in the Austin-Rickett plot for all WMs. The time exponents, *n* of the WMs of lean, standard and super DSSs were determined as 0.20, 0.36 and 0.35, respectively. It follows that precipitation kinetics of γ phase in the reheated WM is also followed by the Austin-Rickett type equation.

The Arrhenius plots of dissolution rate of γ phase in the DSS WMs are shown in Fig.5. The temperature dependency of dissolution rate of γ phase in the reheated WMs of DSSs could be obtained in the present study as follows;

Lean DSS WM:

$$k(T) = \exp\left(\frac{-4.81\times10^4}{T} + 27.8\right) \tag{7}$$

Standard DSS WM:

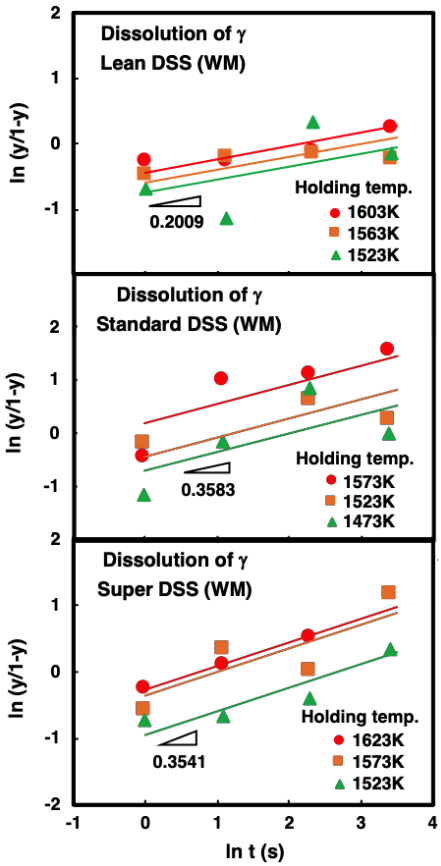


**Fig. 4** Austin-Rickett plots of dissolution behaviour of γ phase in WMs

$$k(T) = \exp\left(\frac{-5.82\times10^{4}}{T} + 37.4\right) \tag{8}$$

Super DSS WM:

$$k(T) = \exp\left(\frac{-4.75\times10^{4}}{T} + 28.8\right) \tag{9}$$

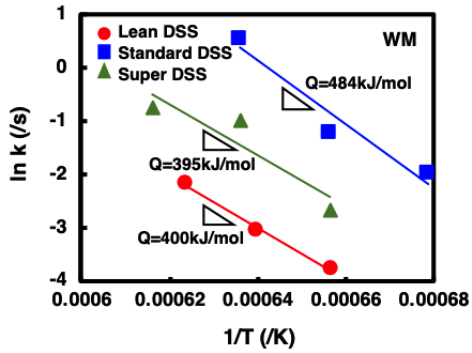


**Fig. 5** Arrhenius plots of dissolution rates of γ phase in WMs

## COMPARISON OF DISSOLUTION RATE BETWEEN HEAT AFFECTED ZONE AND WELD METAL

The dissolution rates of γ phase in the base metal HAZ and reheated WM were compared. Fig.6 shows the temperature dependency of dissolution rate in the HAZ and WM of DSSs. The dissolution of γ phase was enhanced at the higher temperature range in any case. The dissolution rates in the WM of standard and super DSSs were comparable to those in the HAZ, while the dissolution rate in the WM of lean DSS was much reduced to that in the HAZ. The reason why the dissolution rate of lean DSS differed between in the HAZ and WM has not been clarified in the present study, and therefore, the further detailed investigation would be required. In addition, the dissolution rate in the HAZ decreased in the order of lean>standard>super DSSs, *i.e.*, the dissolution of γ phase in the lean DSS HAZ proceeded rapidly compared with the standard and super DSS HAZs.

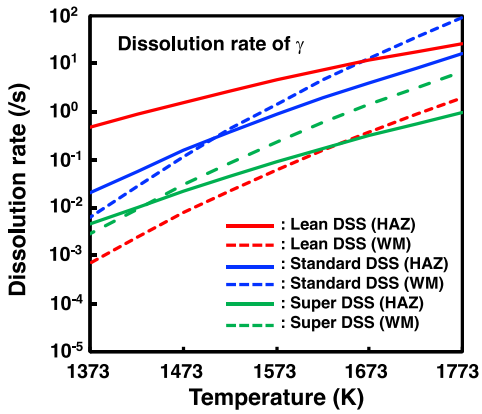


**Fig. 6** Comparison of dissolution rates in HAZ and WM

## PRECIPITATION BEHAVIOUR OF AUSTENITIC PHASE

### PRECIPITATION KINETICS IN BASE METAL HEAT AFFECTED ZONE

The change in microstructure of DSSs during the precipitation treatment was investigated. Fig.7 shows an example of microstructural change (phase mapping by EBSD analysis) in super DSS with the precipitation treatment condition. A γ phase was precipitated not only at the grain boundaries (GBs) (Widmanstätten-like) but also in the grains of α, and the amount of γ phase increased with an increase in the heating temperature. Similar precipitation behaviour has been observed in lean and standard DSSs.

The several researchers have been reported that precipitation kinetics of γ phase in DSS welds was followed by the Austin-Rickett type equation [15-19], and therefore, applicability of the Austin-Rickett type equation to the present precipitation phenomena was verified. Fig.8 shows the Austin-Rickett plots of precipitation behaviour of γ phase in lean, standard and super DSSs. There were good linear relationships in the Austin-Rickett plot, and gradients of the lines were almost identical for all steels. The time exponents *n* of lean, standard and super DSSs were determined as 0.82, 1.16 and 0.53, respectively. It follows that precipitation kinetics of γ phase in the base metal HAZ is also followed by the Austin-Rickett type equation.

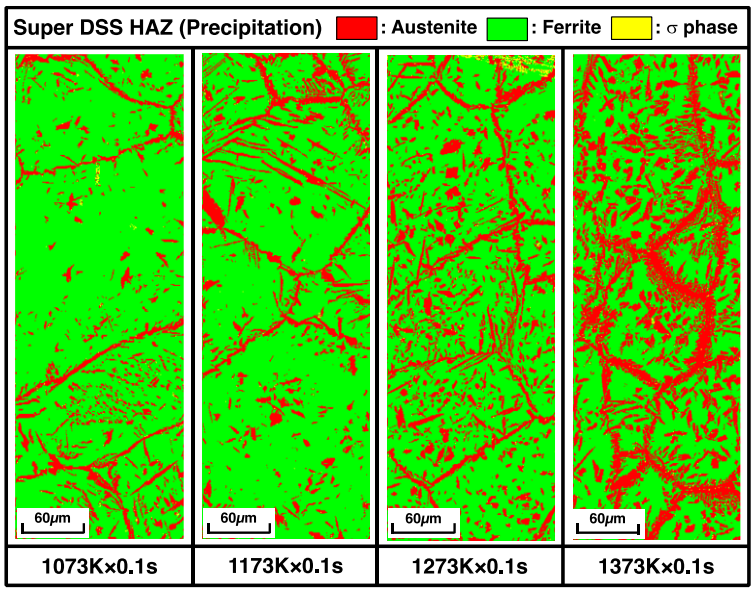


**Fig. 7** Change in microstructure of super DSS with precipitation treatment

According to Fig.8, the precipitation of γ phase in standard and super DSSs was fastest at the heating temperature around 1273 K, while that in lean DSS around 1173 K. The fact that the precipitation of γ phase in DSSs becomes fastest at the certain intermediate temperature (*i.e.*, possesses a "nose") means that the temperature dependency of precipitation rate would not followed by the simple Arrhenius type equation as indicated by eq.(3). Therefore, the temperature dependency of precipitation rate of γ phase in DSSs, which indicates a C-curved diagram with a nose, was theoretically discussed. Assuming that precipitation of γ phase is controlled by the non-uniform nucleation in an α grain and at the α-GB, and grows inward an α grain, the non-uniform nucleation rate $I$ can be expressed by eq.(10) [20];

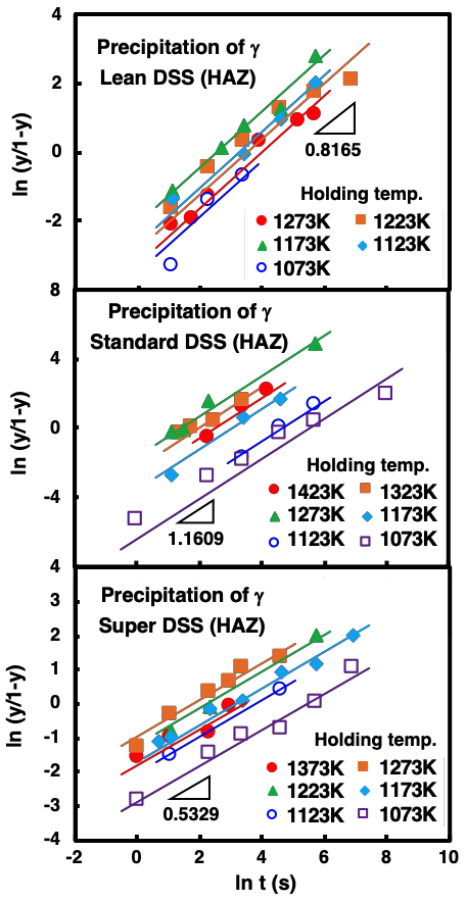


**Fig. 8** Austin-Rickett plots of precipitation behaviour of γ phase in base metal HAZs

$$I = \nu m \left(\frac{d}{L}\right)^{3-j} \exp\left(-\frac{\Delta G^* + \Delta G_a}{RT}\right) \tag{10}$$

where ν is the frequency factor $m$ is the number of atoms per unit volume, $d$ is the effective GB thickness, $L$ is the grain diameter, $j$ is the dimensionality of site, $\Delta G^*$ is the minimum free energy required to form a nucleus, and $\Delta G_a$ is the free energy of activation for a nucleus to continue to grow. Terms in eq.(10) which have temperature dependency are $m$, $L$ and $\Delta G^*$. However, the variation of $m$ is negligible compared with the temperature dependency of exponential term, and $L$ is regarded as constant because the starting specimen is a solution treated specimen at 1653 K for 60 s. Consequently, temperature dependent term in eq.(10) is only $\Delta G^*$, and can be expressed by eq.(11) from the Spherical-Cap model [21];

$$\Delta G^* = \frac{16\pi\sigma_{a/g}^3}{3\Delta G_{V_{a\to g}}^2} f(\theta) \tag{11}$$

where $G_{V_{a\to g}}$ is the volume free energy change from α to γ phase, $\theta$ is the wetting angle of γ phase at the α-GB, and is expressed by the following relationships;

$$G_{V_{a\to g}} = \frac{\Delta H_{a/g}(T_E - T)}{V_m T_E} \tag{12}$$

$$\cos\theta = \frac{\sigma_{a/a} - \sigma_{a/g}}{\sigma_{a/g}} \tag{13}$$

$$f(\theta) = \frac{2 - 3\cos\theta + \cos^3\theta}{4} \tag{14}$$

where $T_E$ is the starting temperature of precipitation of γ phase (γ solvus), $\Delta H_{\alpha/\gamma}$ is the change in enthalpy from α to γ phase at $T_E$, $V_m$ is the molar volume, $\sigma_{\alpha/\alpha}$ and $\sigma_{\alpha/\gamma}$ are the interfacial energies between α and α phases, α and γ phases, respectively. Assuming that $\sigma_{\alpha/\alpha}$ and $\sigma_{\alpha/\gamma}$ are independent on temperature, $\Delta G^*$ in eq.(10) is inversely proportional to the square of degree of undercooling from the starting temperature of precipitation of γ phase, $(T_E\text{-}T)^2$, and expressed by;

$$\Delta G^* = \frac{B^*}{(T_E - T)^2} \tag{15}$$

where $B^*$ is an arbitrary coefficient. Consequently, the non-uniform nucleation rate $I$ in eq.(10) can be expressed by;

$$I = A^* \exp\left(-\frac{\Delta G_a}{RT}\right) \cdot \exp\left\{\frac{-B^*}{RT(T_E - T)^2}\right\} \tag{16}$$

Assuming that the progress in transformation from α to γ phase is controlled by the non-uniform nucleation, the temperature dependency of rate constant $K(T)$ can be also given by;

$$K(T) = A^* \exp\left(-\frac{\Delta G_a}{RT}\right) \cdot \exp\left\{\frac{-B^*}{RT(T_E - T)^2}\right\} \tag{17}$$

where $A^*$ is an arbitrary coefficient. Fig.9 schematically shows the temperature dependency of the rate constant $K(T)$ expressed by eq.(17). The rate constant approaches asymptotically to two types of Arrhenius equation in the temperature ranges below/above a nose.

On the other hand, from the fact that a γ phase in DSS welds grows as the Widmanstätten structure from α-GBs into grains, the precipitation amount of γ phase depends on both nucleation and growth. Namely, the fraction transformed *y* depends on the nucleation rate, diffusion speed and time, and dissolving a diffusion equation assuming the local equilibrium at the α/γ interface, the rate constant $K(T)$ can be approximately expressed by eq.(18) [22];

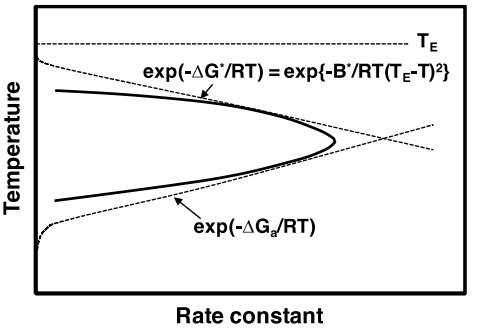


**Fig. 9** Temperature dependency of rate constant

$$K(T) = -\frac{16\sqrt{2}}{15} p D^{2/3} \left( \frac{C_a - C_E}{C_g - C_E} \right) \cdot I \tag{18}$$

where $D$ is the diffusion constant (of N or Ni), $C_\alpha$ and $C_\gamma$ are the solute concentrations (N or Ni) in α and γ phases, respectively, $C_E$ is the equilibrium concentration of solute element (N or Ni) in α phase at the α/γ interface. The diffusion constant can be given by;

$$D = D_0 \exp\left( -\frac{\Delta G_a}{RT} \right) \tag{19}$$

Approximately assuming that $C_\alpha$, $C_\gamma$ and $C_E$ are independent of the temperature and the amount of γ phase (*i.e.*, negligible small compared to the temperature dependency of exponential term), eq.(18) can be transformed to;

$$K(T) = A^{**} \exp\left( -\frac{\Delta G_a}{RT} \right)^{2/3} \cdot \exp\left( -\frac{\Delta G_a}{RT} \right) \cdot \exp\left\{ \frac{-B^*}{RT(T_E - T)^2} \right\} \tag{20}$$

where $A^{**}$ is an arbitrary coefficient. Eq.(20) can be transformed to;

$$K(T) = A^{**} \exp\left( -\frac{5\Delta G_a}{3RT} \right) \cdot \exp\left\{ \frac{-B^*}{RT(T_E - T)^2} \right\} \tag{21}$$

Eq.(21) can be simplified by eq.(22) using three undetermined coefficients $A$, $B$ and $C$;

$$K(T) = A \exp\left( \frac{B}{RT} \right) \cdot \exp\left\{ \frac{C}{RT(T_E - T)^2} \right\} \tag{22}$$

Based on the experimental results (Fig.8), three coefficients (*A*, *B* and *C*) were determined by a regression analysis ($T_E$ can be calculated by the phase computation software, *Thermo-Calc*, Database: TCFE6). Fig.10 shows the temperature dependency of the precipitation rate constants of γ phase in DSSs (regression analysis results of rate constants), and summarises the three coefficients and $T_E$ determined. The precipitation rate of γ phase in DSSs decreased in the order of standard>super>lean DSSs. The temperature dependency of precipitation rate of γ phase in base metal HAZs of DSSs, which indicates a C-curved diagram with a nose, could be obtained in the present study.

## PRECIPITATION KINETICS IN REHEATED WELD METALS

The change in microstructure of the WMs of DSSs during the precipitation treatment was investigated. Fig.11 shows the microstructural change (phase mapping by EBSD analysis) in the WMs of lean, standard and super DSSs with the precipitation treatment condition. A

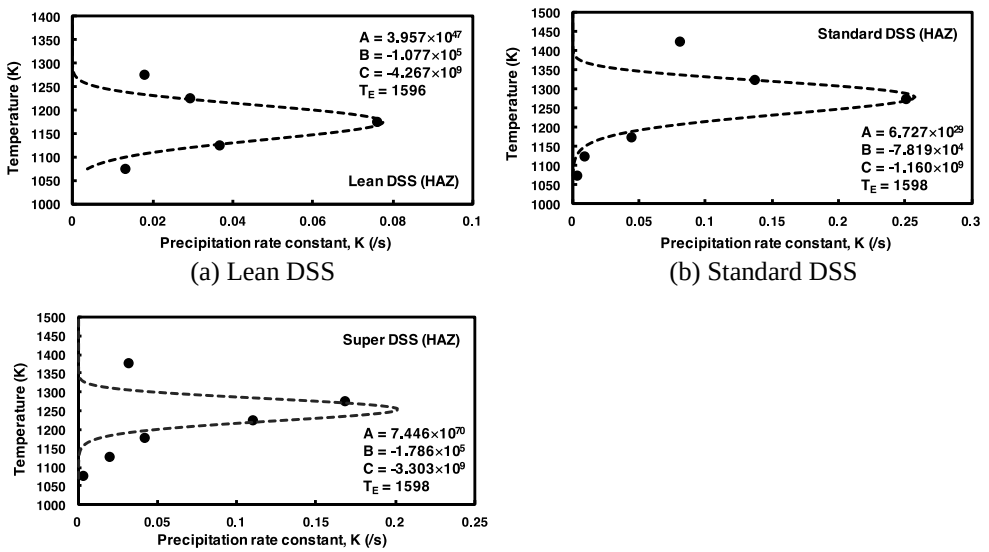


(a) Lean DSS (b) Standard DSS

(c) Super DSS

**Fig. 10** Regression analysis of precipitation rate constants of γ phase in base metal HAZs

γ phase was precipitated in α grains as well as at GBs, and the amount of γ phase increased with an increase in the holding time for all WMs. In addition, very few σ phase was formed in the present conditions.

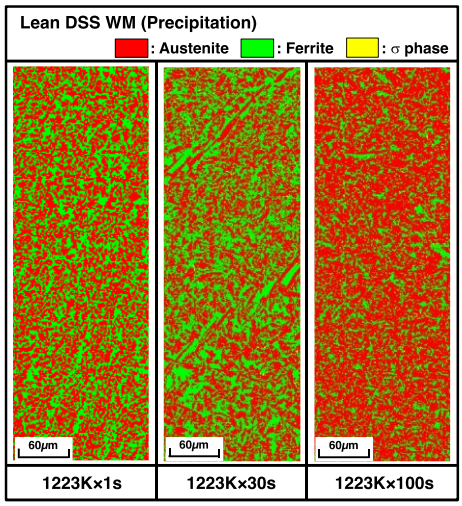


(a) Lean DSS

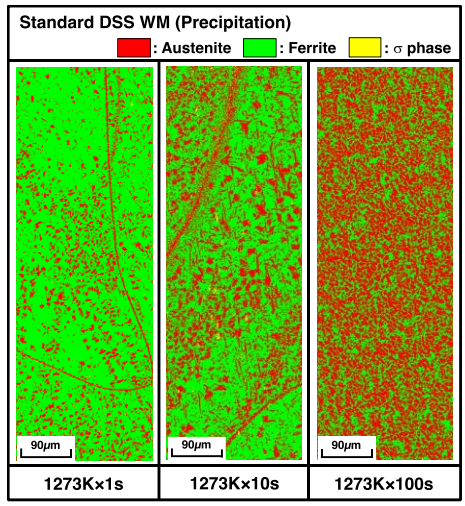


(b) Standard DSS

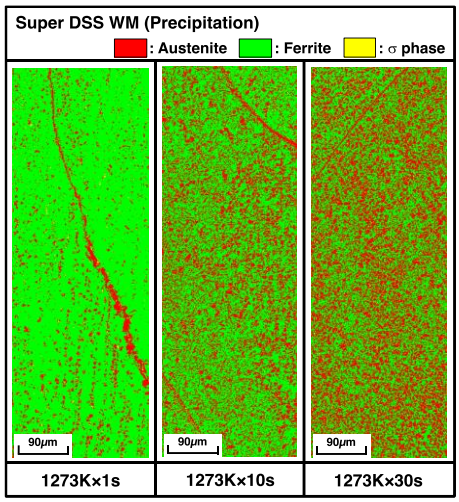


(c) Super DSS

**Fig. 11** Changes in microstructure of DSS WMs with precipitation treatment

The Austin-Rickett plots of precipitation behaviour of γ phase in the WMs of lean, standard and super DSSs are shown in Fig.12. There were good linear relationships in the Austin-Rickett plot again, and gradients of the lines were almost identical for all steels. The time exponents *n* of the lean, standard and super DSS WMs were determined as 0.73, 0.39

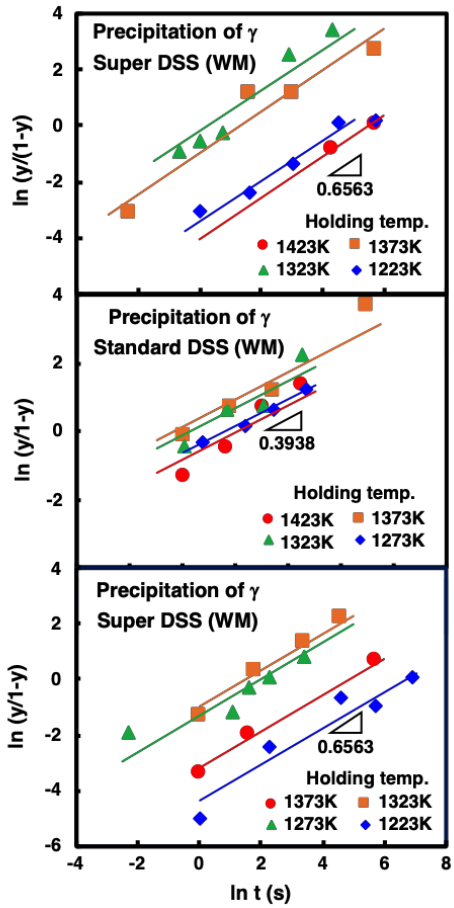


**Fig. 12** Austin-Rickett plots of precipitation behaviour of γ phase in WMs

and 0.66, respectively. The precipitation rates of γ phase in the DSS WMs also possess the temperature dependency with a nose. The nose temperature of precipitation in the standard DSS WM was around 1373 K, while that in super and lean DSSs around 1323 K. It follows that precipitation kinetics of γ phase in the reheated WM is also followed by the Austin-Rickett type equation.

Based on the experimental results (Fig.12), three coefficients (*A*, *B* and *C*) in eq.(22) were determined by a regression analysis again ($T_E$ was calculated by *Thermo-Calc*). Fig.13 shows the temperature dependency of the precipitation rate constants of γ phase in the DSS WMs, and summarises the three coefficients and $T_E$ determined. The precipitation rate of γ phase in DSSs decreased in the order of standard>lean>super DSSs. The temperature dependency of precipitation rate of γ phase in the reheated WMs of DSSs could be also obtained in the present study.

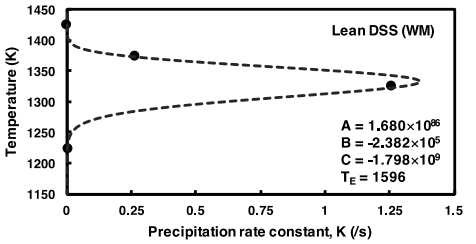


(a) Lean DSS

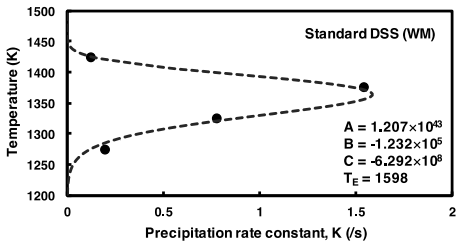


(b) Standard DSS

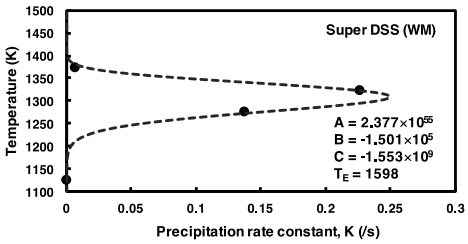


(c) Super DSS

**Fig. 13** Regression analysis of precipitation rate constants of γ phase in WMs

## COMPARISON OF PRECIPITATION RATE BETWEEN HEAT AFFECTED ZONE AND WELD METAL

The precipitation rates of γ phase in the base metal HAZ and reheated WM were compared. Fig.14 shows the temperature dependency of precipitation rate in the HAZ and WM of DSSs. The precipitation rate of γ phase in standard DSS was largest of the three DSSs. The nose temperature and rate constant of the γ phase precipitation in WMs increased compared with those of HAZs in all DSSs. The reason why they differed between the HAZ and WM, especially in lean and standard DSSs, has not been clarified, and therefore, the further detailed investigation would be required.

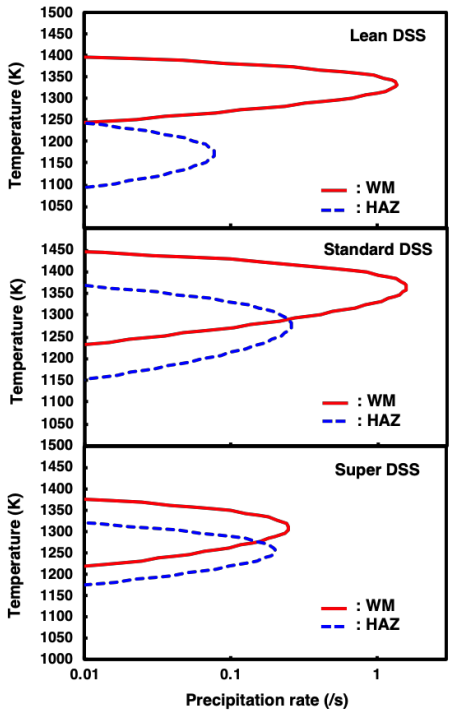


**Fig. 14** Comparison of precipitation rates in HAZ and WM

In order to expand the isothermal kinetics of dissolution and precipitation determined above to the non-isothermal process such as welding, the increment method [18,19] was applied. A concept of the incremental method is that; dividing the thermal cycle into minute isothermal intervals during the $\alpha/\gamma$ phase transformation process, the transformation quantity (increment in the amount of $\gamma$ phase) is calculated in a minute isothermal step, and sum up them through thermal cycle. A flowchart of computation of the phase transformation (the amount of $\gamma$ phase) in multipass welds is shown in Fig.15. The thermal cycles in the HAZ and WM during multipass welding were computed using the welding mechanical analysis software, *JWRIAN*. Compared the $\gamma$ phase fraction at the time to the equilibrium $\gamma$ phase fraction at the temperature in each isothermal step, it was determined that either dissolution or precipitation occurred. Based on the kinetic equations (dissolution and precipitation kinetics) determined, the increment or decrement in the $\gamma$ phase fraction was calculated and summed up through welding process. From these procedures, the alternate behaviours of dissolution and precipitation of $\gamma$ phase during multiple thermal cycle would be numerically simulated. In the present study, the distribution of the $\gamma$ phase fraction in multipass welds was visualised by repeating these calculation over the whole

area of welds (the base metal HAZ and reheated WM). In the previous reports [18,19], the predicted results of the α/γ phase transformation based on the present computation method have been verified in the melt-run welds (GTAW and LBW) of DSSs.

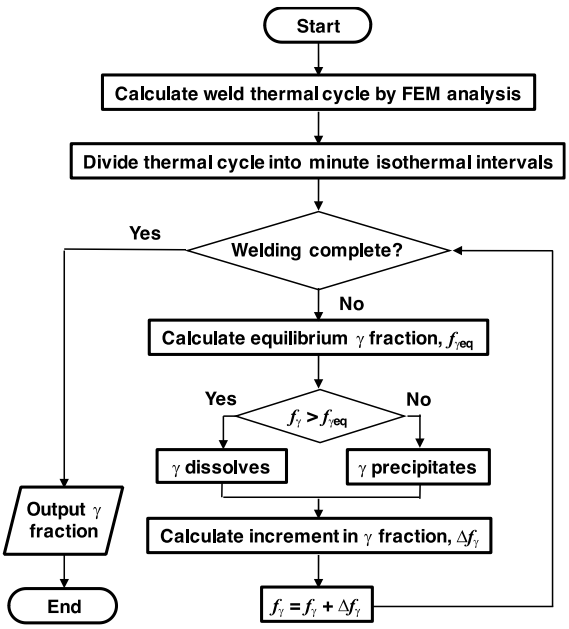


**Fig. 15** Flowchart of computation of phase transformation in multipass welds

Thermal properties of lean, standard and super DSSs [23] used for calculation are shown in Fig.16 (assuming to be identical regardless of the steel grade). The α single-phasing and solidus temperatures of lean, standard and super DSSs, which were calculated by *Thermo-Calc* (Database; TCFE6), are summarised in Table 4. Temperature dependency of the equilibrium γ phase fraction of lean, standard and super DSSs (which was determined based on the measured results combined with the calculated values by *Thermo-Calc* (Database; TCFE6)) is shown in Fig.17. The multipass welding conditions used for computation are described above in EXPERIMENTAL PROCEDURES. In addition, Fig.18 shows the cross-sectional views and mesh division (weld pass sequence) of multipass welds (GTAW) of lean, standard and super DSSs used for numerical analyses of the thermal cycle and α/γ phase transformation (distribution of the γ phase fraction). The total number of weld passes in multipass welding was 15 for all DSSs. The minimum mesh size divided was approx. 0.5 mm × 0.5 mm.

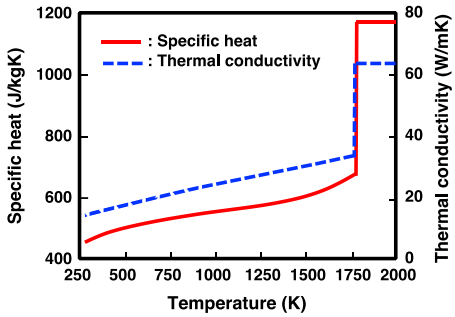


**Fig. 16** Physical properties of DSSs used for calculation

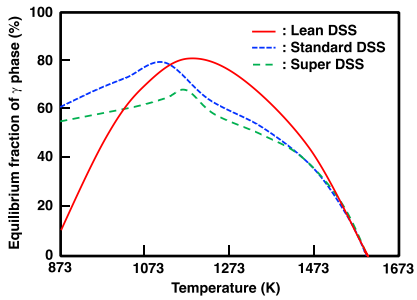


**Fig. 17** Temperature dependency of equilibrium γ phase fraction of DSSs

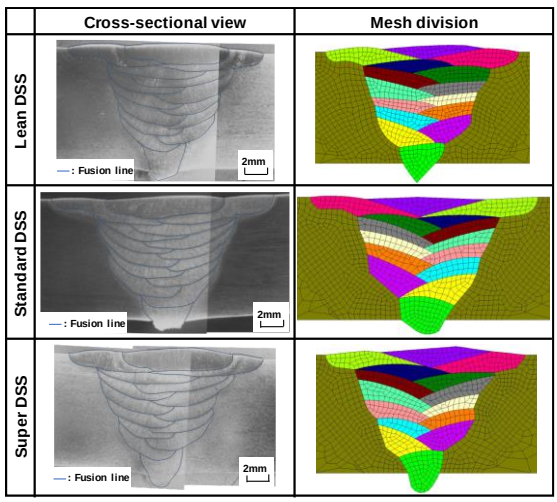


**Fig. 18** Cross-sectional views and mesh division of multipass welds of DSSs

**Table 4** α single-phasing and solidus temperatures of DSSs

| Steel | α single-phasing temp. | Solidus temp. |
|---|---|---|
| Lean DSS | 1596K | 1683K |
| Standard DSS | 1598K | 1647K |
| Super DSS | 1598K | 1604K |

COMPUTED RESULTS OF AUSTENITIC PHASE FRACTION IN WELDS

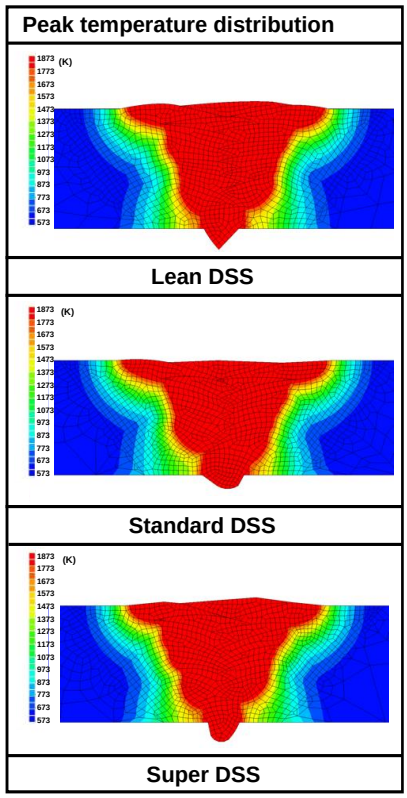


**Fig. 19** Peak temperature distribution in multipass welds of DSSs

The thermal cycles during multipass GTA welding (the number of weld passes is 15) of DSSs were calculated. Fig.19 shows the peak temperature distribution in the base metal HAZs of lean, standard and super DSSs during multipass welding computed by the heat conduction analysis using *JWRIAN*. The peak temperature distribution and thermal cycle in multipass welds could be successfully computed for all DSSs. Based on the multiple thermal cycles calculated in the base metal HAZs and reheated WMs, the α/γ phase transformation in multipass GTA welds of DSSs was computed. Fig.20 shows the distribution of the γ phase fraction (indicated by colour contours) calculated in the multipass weld of lean DSS. This figure exhibits the entire history of the distribution of the γ phase

fraction at the completion of each weld pass during multipass welding. The dashed lines in the figure indicate the fusion lines of weld passes. The γ phase fraction in the just solidified WM was considerably small in any weld passes, and the depleted zone of γ phase was formed adjacent to the fusion line ("under-bead" region) in the base metal HAZs and reheated WMs. However, the γ phase fraction in the depleted zone was increased by the subsequent weld passes (the γ phase was re-precipitated by the thermal cycles in subsequent welding). Accordingly, the α/γ phase balance has been complexly varied in multipass welds, and the profile of the γ phase fraction was arranged in laminae in the WM roughly along the fusion lines. The minimum γ phase fraction in multipass welds was approx. 20% located in the base metal HAZ of the final weld layer, and the γ phase fraction in WMs was reduced to approx. 25%. On the other hand, the γ phase fraction in a part of base metal HAZ (low temperature HAZ) was exceeded to that in the base metal, because of the additional precipitation of γ phase during multipass welding. The distribution of the γ phase fraction calculated in the multipass welds of standard and super DSSs is also shown in Fig.21 and Fig.22, respectively. Quite similar tendencies to lean DSS weld were observed in the distribution of the γ phase fraction, that is, the γ phase fraction was reduced in the solidified WM and under-bead region of WM as well as the base metal HAZ, while the γ phase fraction in the depleted zone was recovered by the subsequent weld passes. As a result, the α/γ phase balance has been complexly varied in multipass welds. Furthermore, the γ phase fraction in multipass weld (especially WM) of standard DSS was slightly lower than those of lean and super DSSs, namely, the γ phase fraction in standard DSS weld was reduced to approx. 10-15%, while those in lean and super DSS welds were reduced to approx. 25-30%. On the other hand, the over-precipitated zone, where the γ phase fraction slightly exceeded the base metal level, was not observed in the low temperature HAZ of standard DSS weld, whereas it was observed in other welds.

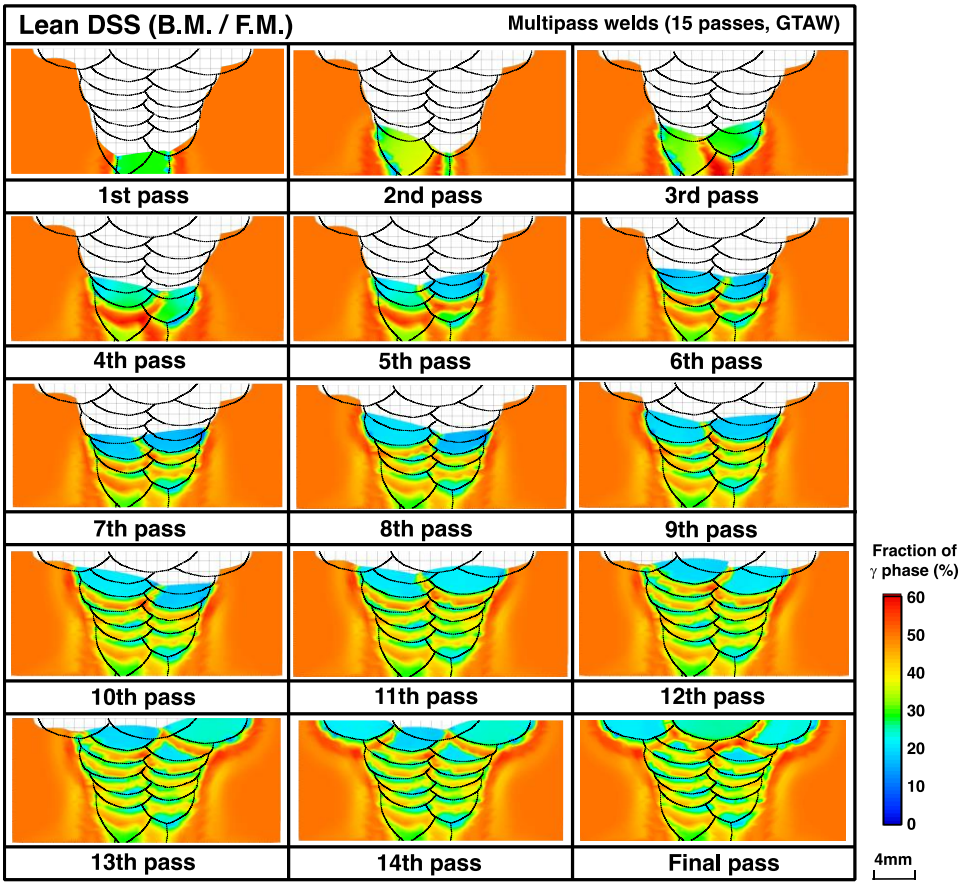


**Fig. 20** Distribution of γ phase fraction calculated in multipass weld of lean DSS

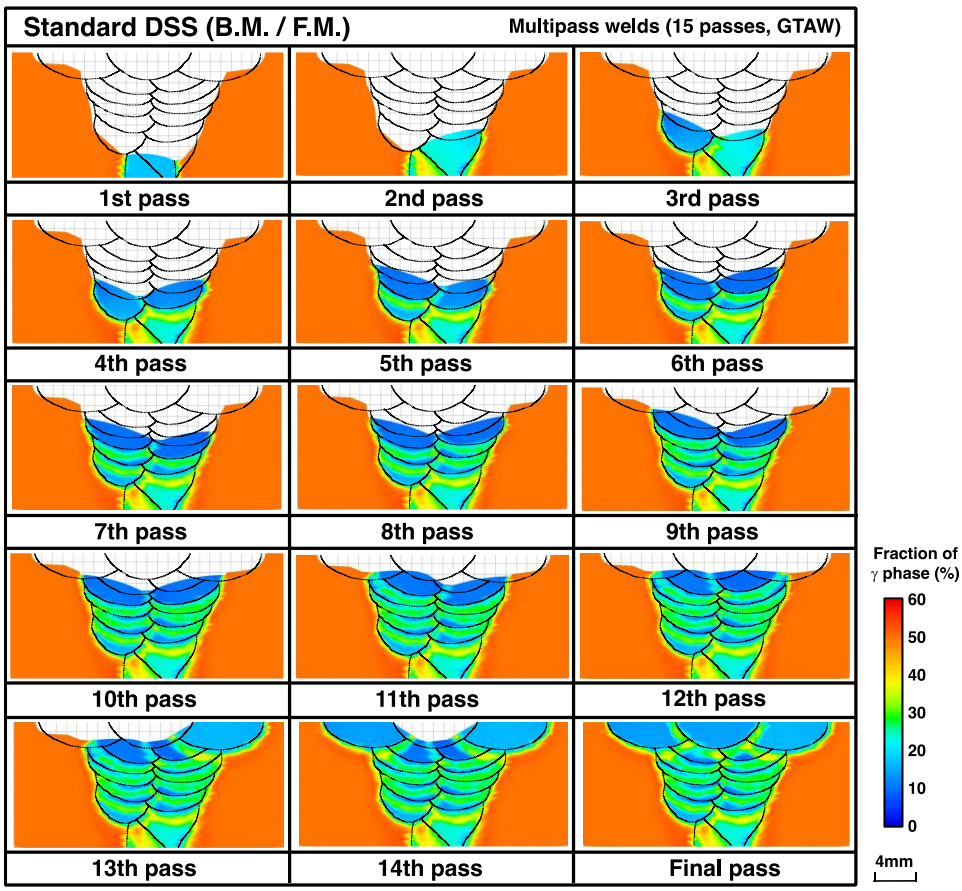


**Fig. 21** Distribution of γ phase fraction calculated in multipass weld of standard DSS

## COMPARISON OF AUSTENITIC PHASE FRACTION IN MULTIPASS WELDS BETWEEN CALCULATED AND MEASURED

In order to validate the predicted results of the α/γ phase transformation, the γ phase fraction in the multipass welds was compared between calculated and measured. Fig.23 shows the example of microstructure (phase mapping by EBSD analysis) of multipass welds. This figure shows the microstructure of lean, standard and super DSSs observed at the final weld layer in multipass welding as schematically shown in Fig.24. A dashed line in Fig.23 indicates the fusion line. The γ phase fraction was relatively reduced in the higher temperature HAZ (base metal HAZ) as well as WM of all steels. In particular, the γ phase

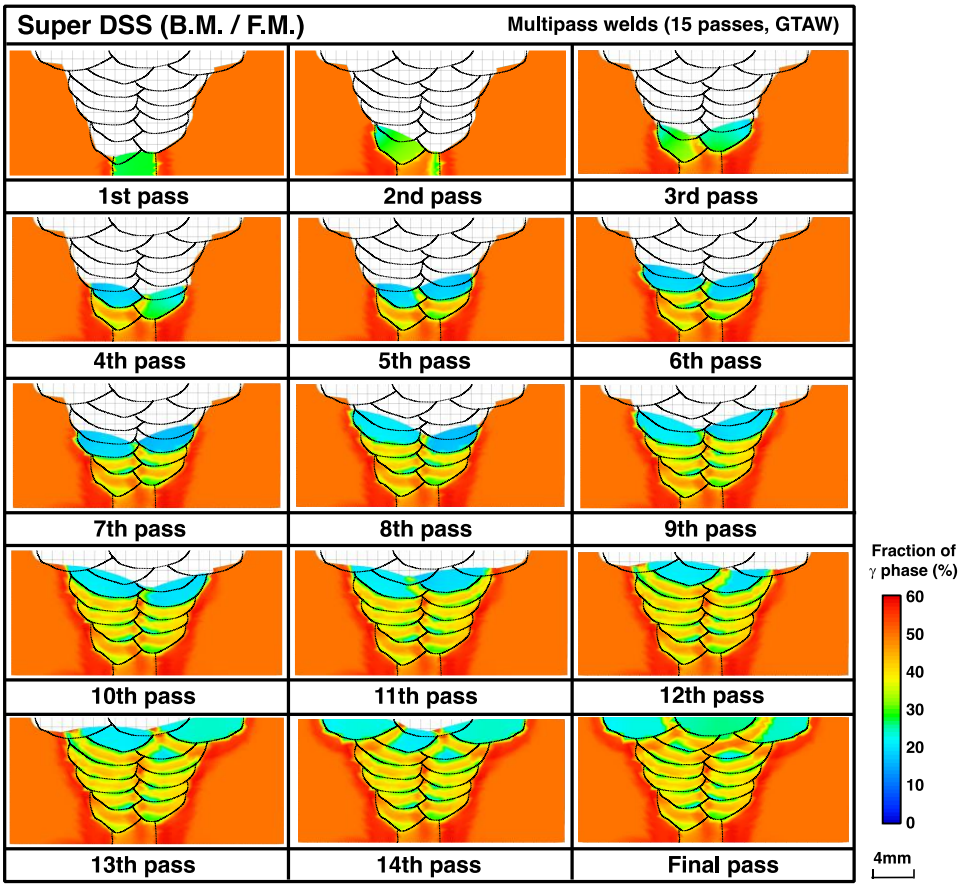


**Fig. 22** Distribution of γ phase fraction calculated in multipass weld of super DSS

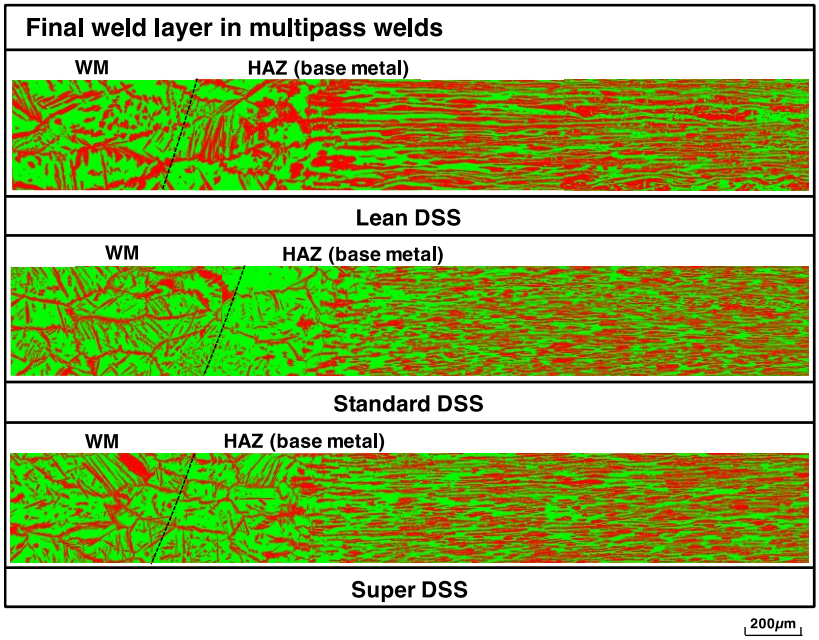


**Fig. 23** Microstructures of final layer (WM and HAZ) in multipass welds

fraction in the HAZ of standard DSS was much reduced compared to other steels. The γ phase fraction at the various positions was measured in multipass welds. Figs.25-27 show the comparison of the γ phase fraction between calculated and measured in the multipass welds (GTAW) of lean, standard and super DSSs, respectively. In these figures, a figure (a) indicates the analysis spots (positions) of the γ phase fraction, and a figure (b) indicates the correlation between the calculated γ phase fraction and measured one. The analysis spots were dotted across the welds in the reheated/un-reheated WMs and base metal HAZ. Although there were small scatters between the calculated and measured values, the calculated results were fairly consistent with measured ones (correlation coefficients; 0.81-

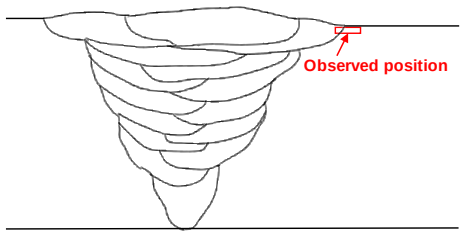


**Fig. 24** Observed position of microstructure in multipass weld

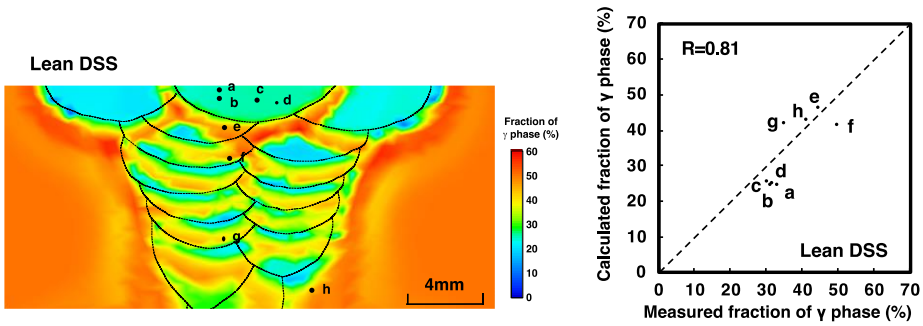


(a) Analysis spots (b) Correlation of γ phase fraction

**Fig. 25** Comparison of γ phase fraction between calculated and measured in lean DSS multipass weld

0.90) in all welds (in the WM, reheated WM as well as the base metal HAZ). It follows that the α/γ phase transformation in the DSS multipass welds could be successfully predicted by the present kinetic approach and computer simulation. In particular, the γ phase-depleted zone in the multipass welds, where the mechanical and corrosion properties would be potentially deteriorated, could be estimated with a high degree of accuracy.

## CONCLUSIONS

In the present study, the kinetic approach was made to the α/γ phase transformation phenomena in the multipass welds of DSSs. Both of the dissolution and precipitation

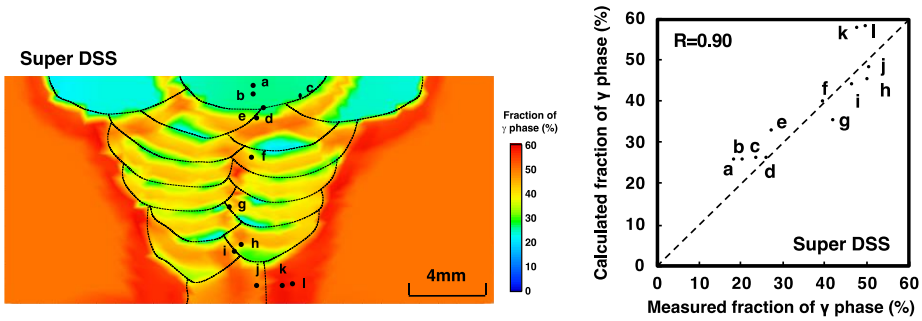


(a) Analysis spots (b) Correlation of γ phase fraction

**Fig. 26** Comparison of γ phase fraction between calculated and measured in super DSS multipass weld

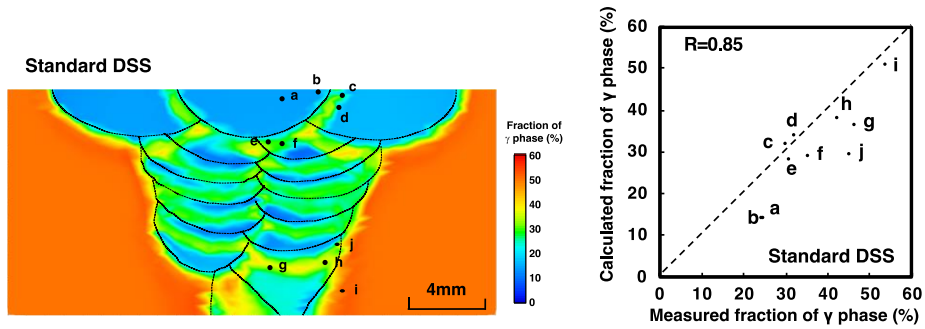


(a) Analysis spots (b) Correlation of γ phase fraction

**Fig. 27** Comparison of γ phase fraction between calculated and measured in standard DSS multipass weld

behaviours of γ phase were kinetically investigated for the reheated WM as well as the base metal HAZ, and the γ phase fraction in multipass welds of DSSs was numerically calculated by coupling with the heat conduction analysis during multipass welding. Finally, the predicted results of α/γ phase transformation in multipass welds were verified by the experimental examination. The results obtained are summarised as follows;

(1) The dissolution and precipitation kinetics of γ phase in the base metal HAZ and WM were followed by the Austin-Rickett type equation.

(2) The temperature dependency of the dissolution and precipitation rates of γ phase was determined. The dissolution rate in the HAZ of lean DSS was slightly larger than those in the HAZs of standard and super DSSs. The precipitation rate of γ phase in standard DSS was largest of the three DSSs. The nose temperature and rate constant of the γ phase precipitation in WMs increased compared with those of HAZs in all DSSs.

(3) Based on the kinetic equations determined, the distribution of the γ phase fraction in multipass welds of DSSs was calculated combined with the heat conduction analysis in welding process. The incremental method was applied to expand the dissolution and precipitation kinetics to the non-isothermal process. The γ phase fraction in the just solidified WM was considerably small in any weld passes, and the depleted zone of γ phase was formed in the “under-bead” region in the base metal HAZs and reheated WMs. However, the γ phase fraction in the depleted zone was increased (recovered) by the subsequent weld passes.

(4) The γ phase fraction in multipass weld of standard DSS was slightly lower than those of lean and super DSSs. The over-precipitated zone, where the γ phase fraction slightly exceeded the base metal level, was not observed in the low temperature HAZ of standard DSS weld, whereas it was observed in other welds.

(5) Microstructural observation revealed that the calculated results of γ phase fraction in multipass welds were consistent with experimental ones. It followed that the α/γ phase transformation in DSS welds could be successfully predicted by the present approach.

## ACKNOWLEGEMENTS

The authors would like to thank Messrs. Y. Tanabe and J. Tokunaga (Osaka Univ.) for their cooperation in this research.

## REFERENCES

[1] M.MIURA, M.KOSO, T.KUDO AND H.TSUGE: 'Effect of Nickel and Nitrogen on Microstructure and Corrosion Resistance of Duplex Stainless Steel Weldment', *Quarter. J. JWS*, Vol.7 No.1 (1989), p.94-100 (in Japanese).

[2] O.KAMIYA, K.KUMAGAI, T.ENJO AND Y.KIKUCHI: 'Effect of Microstructure on Fracture Toughness of SUS329J1 Duplex Stainless Steel Welds', *Quarter J. JWS*, Vol.8 No.1 (1990), p.105-111 (in Japanese).

[3] N.A.MCPHERSON, Y.LI AND T.N.BAKER: 'Microstructure and Properties of As Welded Duplex Stainless Steel', *Sci. & Technol. Welding & Joining*, Vol.5 No.4 (2000), p.235-244.

[4] R.BADJI, M.BOUABDALLAH, B.BACROIX, C.KAHLOUN, B.BELKESSA AND H.MAZA: 'Phase Transformation and Mechanical Behavior in Annealed 2205 Duplex Stainless Steel Welds', *Mater. Characterization*, 59 (2008), p.447-453.

[5] J.W.ABTIBOL MENEZES, H.ABREU, S.KUNDU, H.K.D.J.BHADESHIA AND P.M.KELLY: 'Crystallography of Widmanstätten Austenite in Duplex Stainless Steel Weld Metal', *Sci. & Technol. Welding & Joining*, Vol.14 No.1 (2009), p.4-10.

[6] R.J.RAMIREZ, S.D.BRANDI AND J.C.LIPPOLD: 'Secondary Austenite and Chromium Nitride Precipitation in Simulated Heat Affected Zones of Duplex Stainless Steels', *Sci. & Technol. Welding & Joining*, Vol.9 No.4 (2004), p.301-313.

[7] J.-O.NILSSON, T.HUHTALA, P.JONSSON, L.KARLSSON AND A.WILSON: 'Structural Stability of Super Duplex Stainless Weld Metals and Its Dependence on Tungsten and Copper', *Metall. Mater. Trans.*, Vol.27A No.10 (1996), 2196-2208.

[8] R.BADJI, M.BOUABDALLAH, B.BACROIX, C.KAHLOUN, K.BETTAHAR AND N.KHERROUBA: 'Effect of Solution Treatment Temperature on the Precipitation Kinetic of σ-Phase in 2205 Duplex Stainless Steel Welds', *Mater. Sci. Eng.*, A 496 (2008), p.447-454.

[9] K.NISHIMOTO, K.SAIDA AND O.KATSUYAMA: 'Prediction of Sigma Phase Precipitation in Super Duplex Stainless Steel Weldments', *Welding in the World*, Vol.50 No.3/4 (2006), p.13-28.

[10] S.H.WANG, P.K.CHIU, J.R.YANG AND J.FANG: 'Gamma (γ) Phase Transformation in Pulsed GTAW Weld Metal of Duplex Stainless Steel', *Mater. Sci. Eng.*, A 420 (2006), p.26-33.

[11] H.LIU AND X.JIN: 'Secondary Austenite Morphologies in Fusion Zone of Welded Joint after Postweld Heat Treatment with a Continuous Wave Laser', *J. Mater. Sci. Technol.*, Vol.28 No.3 (2012), p.249-254.

[12] T.A.PALMER, J.W.ELMER AND J.WONG: 'In Situ Observation of Ferrite-Austenite Transformations in Duplex Stainless Steel Weldments using Synchrotron Radiation', *Sci. & Technol. Welding & Joining*, Vol.7 No.3 (2002), p.159-171.

[13] C.M.GARZÓN AND A.J.RAMIRES: 'Growth Kinetics of Secondary Austenite in the Welding Microstructure of a UNS S32304 Duplex Stainless Steel', *Acta Mater.*, Vol.54 (2006), p.3321-3331.

[14] D.J.KOTECKI: 'Ferrite Control in Duplex Stainless Steel Weld Metal', *W.J.*, Vol.65 No.10 (1986), p.273s-278s.

[15] Y.NAKAO, K.NISHIMOTO AND S.INOUE: 'Kinetics of the Formation of Austenite at Constant Temperature, -Study on the Phase Transformation in Welded Joints of Duplex Stainless Steels (Report 1)-', *J. JWS*, Vol.50 No.5 (1981), p.514-520 (in Japanese).

[16] Y.NAKAO, K.NISHIMOTO AND S.INOUE: 'Quantitative Analysis of Austenite Formation in HAZ, -Study on the Phase Transformation in Welded Joints of Duplex Stainless Steels (Report 2)-', *J. JWS*, Vol.50 No.11 (1981), p.1107-1111 (in Japanese).

[17] K.YASUDA, R.N.GUNN AND T.G.GOOCH: 'Prediction of Austenite Phase Fraction in Duplex Stainless Steel Weld Metals', *Quarter. J. JWS*, Vol.20 No.1 (2002), p.68-77 (in Japanese).

[18] K.SAIDA, K.NISHIMOTO, H.INOUE AND Y.OIKAWA: 'Prediction of Phase Transformation in Duplex Stainless Steel Welds', *Mathematical Modelling of Weld Phenomena 11*, ed. by C.Sommitsch, N.Enzinger and P.Mayr, (2016), p.109-122.

[19] T.OGURA, Y.TANABE, H.INOUE, Y.OIKAWA AND K.SAIDA: 'Kinetics of Phase Transformation in Weld Heat Affected Zone of Duplex Stainless Steels', 9th European Stainless Steel Conference - Science & Market (ESSC2017) & 5th European Duplex Stainless Steel Conference & Exhibition (DUPLEX 2017), 21-23rd May (2017), Bergamo (Italy).

[20] J.W.CAHN: 'The Kinetics of Grain Boundary Nucleated Reactions', *Acta Metall.*, Vol.4, (1956), p.449-459.

[21] W.C.JOHNSON, C.L.WHITE, P.E.MARTH, P.K.RUF, S.M.TUOMINEN, K.D.WADE, K.C.RUSSELL AND H.I.AARONSON: 'Influence of Crystallography on Aspects of Solid-Solid Nucleation Theory', *Metall. Trans. A*, Vol.6A No.4 (1975), p.911-919.

[22] K.HIRANO: 'GOUKIN NO GIKOU KATEI TO SONO KAISHAKU', KINZOKUGAKKAI SEMINAR, (1968), p.1-28 (in Japanese).

[23] J.J.DEL COZ DIAZ, P.MENENDEZ RODRIGUEZ, P.J.GARCIA NIETO AND D.CASRO-FRESNO: 'Comparative Analysis of TIG Welding Distortions between Austenitic and Duplex Stainless Steels by FEM', *Applied Thermal Eng.*, Vol.30, (2010), p.2448-2459.